Collisionless plasma expansion into vacuum: two new twists on an old problem

Alexey V. Arefiev and Boris N. Breizman

Institute for Fusion Studies, The University of Texas, Austin, Texas 78712

(Dated: December 12, 2008)

Abstract

The paper deals with a generic problem of collisionless plasma expansion into vacuum in the regimes where the expanding plasma consists of hot electrons and cold ions. The expansion is caused by electron pressure and serves as an energy transfer mechanism from electrons to ions. This process is often described under the assumption of Maxwellian electrons, which easily fails in the absence of collisions. The paper discusses two systems with a naturally occurring non-Maxwellian distribution: an expanding laser-irradiated nanoplasma and a supersonic jet coming out of a magnetic nozzle. The presented rigorous kinetic description demonstrates how the deviation from the Maxwellian distribution fundamentally alters the process of ion acceleration during plasma expansion. This result points to the critical importance of a fully kinetic treatment in problems with collisionless plasma expansion.

I. INTRODUCTION

Plasma expansion into a vacuum is a basic physics problem with a variety of applications, ranging from solar wind to laboratory plasmas [1–5]. It has been extensively studied over the years [6–13], but recent research of laser irradiated nanoplasmas [14] and plasma based space thrusters [15] reveal interesting new elements in this seemingly transparent problem. This paper presents two such elements involving kinetic phenomena.

We focus specifically on the regimes where the plasma consists of hot electrons and cold ions. In these regimes the expansion is driven by the electron pressure, and it serves as an energy transfer mechanism from electrons to ions. If the electron motion is collisional, then the process is largely similar to the conventional gas-dynamic expansion [16] with the fluid description fully applicable [17]. In this case the electron distribution remains Maxwellian during the expansion due to the Coulomb electron-electron collisions. Plasma expansion with collisionless electrons is also often treated under the assumption that the electrons are Maxwellian [6, 9, 18], but this approach generally suffers from the lack of a mechanism capable of maintaining such a distribution. In some special cases this assumption can be justified by proving that the obtained solution is internally consistent despite the absence of collisions or any other Maxwellization mechanism [6, 13]. However, these special cases are rare exceptions because the expansion itself can easily distort an initially Maxwellian distribution in the absence of collisions. Moreover, the electron distribution prior to the expansion may already be significantly different from a Maxwellian. Both situations apparently require a proper first-principle kinetic treatment.

This paper considers two systems with intrinsically non-Maxwellian electron distributions: an expanding laser-irradiated nanoplasma and a supersonic jet coming out of a magnetic nozzle. Our rigorous kinetic analysis of these two problems (Secs. II and III) demonstrates how the deviation from the Maxwellian distribution fundamentally alters ion acceleration compared to a model that postulates a Maxwellian electron distribution in the entire flow. The problem of a laser-irradiated nanoplasma highlights the critical role of hot non-thermal electrons in the ion acceleration process. A detailed kinetic analysis of this problem is presented in Ref. [14], whereas Sec. II serves as an overview of the key qualitative results of Ref. [14]. The magnetic nozzle problem shows the important role of the moving plasma edge in the distortion of the electron distribution.

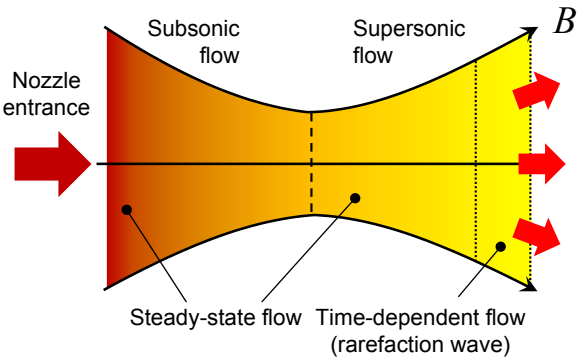

FIG. 1: Plasma flow in a magnetic nozzle with a converging-diverging guiding magnetic field configuration.

Most of the paper is dedicated to the problem of plasma acceleration in a magnetic nozzle with a converging-diverging configuration of the guiding magnetic field. This configuration is employed by some plasma-based propulsion concepts to convert an incoming subsonic plasma flow into a supersonic jet. The converging part of the nozzle accelerates the incoming subsonic flow supplied by a plasma source. The flow becomes sonic at the nozzle throat, after which the acceleration continues in the diverging part of the nozzle. The main difference from a convention gas-dynamic nozzle is that the flow acceleration mechanism is collisionless. The electron pressure produces an ambipolar electric field directed downstream that pulls the ions, accelerating the flow.

At a constant rate of plasma injection, the flow upstream from the nozzle throat (magnetic mirror) and in its vicinity downstream eventually reaches a steady state. The expanding plume, however, remains time dependent and consists of two parts: a steady supersonic flow adjacent to the mirror and a rarefaction wave at the plasma edge (see Fig. 1). This flow configuration is similar to that of a conventional gas-dynamic nozzle, but there is a fundamental difference. The rarefaction wave at the plasma edge affects the flow globally through collisionless electrons, as opposed to the collisional flow regime where it affects electrons only locally due to the short electron mean free path.

The magnetic mirror makes some areas of phase space inaccessible to the electrons injected by the source because only those electrons in the loss cone upstream from the mirror are able to pass through. These areas were treated as empty in previous works when attempting to construct a steady-state solution for a collisionless flow [18]. Such an approach unjustifiably ignores electron interaction with the rarefaction wave. A critical aspect of this interaction

is the energy loss caused by the time-dependent electric field of the wave. Its consequence is that some of the reflected electrons do not have sufficient energy to overcome the barrier created by the magnetic mirror and return to the plasma source. These electrons become decoupled from the source and undergo continuous adiabatic cooling, bouncing between the mirror and the rarefaction wave. As a result, the inaccessible areas of phase space downstream from the mirror become filled with decoupled electrons.

In Sec. III of this paper, we formulate a closed set of equations that adequately describes the collisionless plasma plume for a given distribution of injected electrons. The decoupled electrons affect the description in a major way. The derived equations are solved for the case of injected Maxwellian electrons to demonstrate the distortion of the electron distribution and the resulting significant change in ion acceleration compared to a model that postulates Maxwellian electrons in the entire flow.

II. ION ACCELERATION IN EXPANDING NANOPLASMAS

This section describes collisionless expansion of a nanoplasma (micro-cluster) with a two-component electron distribution. The corresponding theory has been largely motivated by experimental studies of micro-clusters that are exposed to a high-intensity laser beam [4]. In a typical experiment, a supersonic deuterium jet expands into vacuum producing liquid-density droplets, which are a few nanometers in radius. When the droplets are irradiated with an intense laser pulse, they are quickly converted into dense fully ionized nanoplasmas (micro-clusters). The nanoplasmas expand producing counter-streaming fluxes of fast ions and subsequent ion collisions lead to fusion reactions with a noticeable neutron yield [4]. Quantitative predictions of the neutron yield require the knowledge of the ion spectrum and understanding of the expansion dynamics.

The problem involves two elements that can be considered as subsequent stages in a short laser pulse limit when the pulse duration is significantly shorter than the cluster expansion time. The first stage is the electron heating by the laser, and there are several possible regimes depending on the electron mean free path, cluster radius, and laser pulse parameters. The regime of particular interest for theory is the one where the laser can create a two-component electron distribution with a cold majority and a hot collisionless minority. The underlying mechanism is the so-called Brunel heating [19, 20] that takes place at the cluster

surface and repeats stochastically during multiple passes of the heated electron through the cluster [21–24] . The second stage is the ion acceleration which, in this limit, is a problem of plasma expansion into vacuum for a given initial electron distribution. The mechanism of electron heating by the laser is such that the hot electrons move predominantly radially, which makes the problem of ion expansion caused by the hot electron pressure effectively one-dimensional.

The key feature of the problem is that both cold and hot electron populations occupy the same volume prior to the expansion. Such initial configuration is the cause for the breakdown of quasineutrality at the edge of the cold electron core during the expansion. A detailed analysis of the expansion dynamics is given in Ref. [14], and in what follows we summarize its results. Initially all ions and both electron populations occupy the same volume inside the cluster where the sum of the electron densities is equal to the ion density, so that the charge density and electric field vanish. There is also a thin double layer at the cluster surface (the same as the surface of the cold electron core) that consists of a negatively charged hot electron halo and a positively charged ion shell. The electric field of the double layer keeps hot electrons inside the cluster but, at the same time, it forces the ions of the thin shell to expand radially. As the original ions from the thin shell expand, new ions become exposed to the electric field of the double layer. Gradually, a new double layer structure shown in Fig. 2 is formed at the surface of the cold electron core. It is critical that the ions are extracted from inside the cluster where the ion density significantly exceeds the hot electron density. Therefore, continuous violation of quasineutrality is unavoidable at the edge of the cluster, so that the double layer must persist during hot electron expansion.

The double-layer shown in Fig. 2 produces a quasineutral outgoing supersonic plasma flow. The drop of the electrostatic potential in the double layer is insufficient to confine all hot electrons inside the cluster. The remaining drop of the electrostatic potential needed to reflect back all the hot electrons that are moving radially outwards is accommodated by a rarefaction wave at the expanding plasma edge. A self-consistent theory that describes ion expansion together with the resulting cooling of the hot electrons has been developed in Ref. [14] for a top-hat distribution of the hot electron component. The rigorous solution of the problem allows one to find asymptotic ($t \to +\infty$) ion energy and time-of-flight spectra. These spectra indicate that the average ion energy gain is of the order of the hot electron energy before the expansion and that there is a fraction of ions whose maximum energy

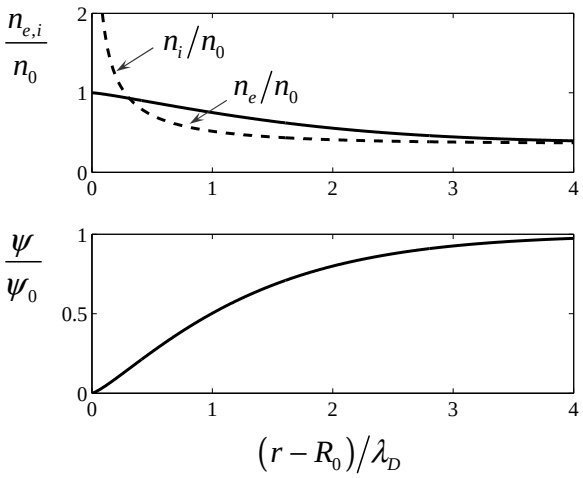

FIG. 2: Electron and ion density profiles (n_e and n_i) and electrostatic potential (ψ) in the double layer. The densities are normalized to the hot electron density n_0 at the surface of the cold electron core. The surface of the cold electron core is located at $r = R_0$. The electrostatic potential is normalized to its value at the double layer exit $\psi_0 = -\sqrt{3\mathcal{E}_H/2|e|}$, where $\mathcal{E}_H$ is the maximum (cutoff) electron energy. The radial scale is normalized to $\lambda_D = \sqrt{\mathcal{E}_H/4\pi n_0 e^2}\left[\mathcal{E}_H^{t=0}/\mathcal{E}_H\right]^{1/4}$.

exceeds the initial maximum electron energy. It also follows from the solution that the ions gain as much as 50% of their final energy moving through the double layer located at the surface of the cold electron core.

III. EXPANSION OF SUPERSONIC PLASMA JET

The qualitative picture of expansion of a supersonic plasma jet into vacuum was discussed recently in Ref. [15]. In what follows, we adopt the same general formulation of the problem and reduce introductory qualitative arguments to the bare minimum with the understanding that more details can be found in Ref. [15].

We consider a collisionless paraxial plasma flow through an axisymmetric magnetic nozzle with a steady plasma source at the nozzle entrance (a source with a constant rate of plasma injection). The incoming flow is subsonic and the plasma ions are assumed to be cold and single-charged. The dynamics of such a flow is described by the following equations:

$$\frac{\partial V}{\partial t} + V\frac{\partial V}{\partial z} = -\frac{|e|}{m_i}\frac{\partial \varphi}{\partial z}, \tag{1}$$

$$\frac{\partial n}{\partial t} + B\frac{\partial}{\partial z}\left(\frac{nV}{B}\right) = 0, \tag{2}$$

$$n = n_e(\varphi, B), \tag{3}$$

where V is the ion velocity that is directed along the given guiding magnetic field $B(z)$, m_i is the ion mass, e is the electron charge, φ is the electrostatic potential, n is the ion density, n_e is the electron density, z is the axial coordinate, and t is the time. Equation (1) is the ion momentum balance equation, Eq. (2) is the ion continuity equation, and Eq. (3) is the quasineutrality condition. The electron density in Eq. (3) must be expressed in terms of φ, B, and a given distribution function of injected electrons f_0.

The motion of plasma electrons is controlled by the guiding magnetic field $B(z)$ and the ambipolar potential $\varphi(z;t)$. The nozzle concept implies that the electrons are strongly magnetized, such that they follow the magnetic field lines. The time evolution of φ is determined by the ion motion and can be regarded as slow (adiabatic) with respect to the electron gyromotion and electron axial motion. Therefore, the magnetic moment of each electron,

$$\mu \equiv \frac{m_e v_\perp^2}{2B}, \tag{4}$$

is a conserved quantity, where m_e is the electron mass and $v_\perp$ is the electron velocity perpendicular to the magnetic field. The electron motion along the field lines can then be described as one-dimensional motion in an effective potential

$$U_{\text{eff}} \equiv \mu B(z) - |e|\varphi(z;t). \tag{5}$$

We assume that the ambipolar potential φ is a monotonically decreasing function of the axial coordinate z, so that plasma ions accelerate progressively along the magnetic field lines. In contrast with $\varphi(z)$, the effective potential U_{eff} is not monotonic for electrons with a sufficiently high μ and it has a local maximum downstream from the magnetic mirror because of the magnetic term in Eq. (5). The location of the maximum depends on the electron magnetic moment.

We distinguish two groups of electrons: coupled electrons and decoupled electrons. Coupled electrons are the electrons that return to the plasma source after a single axial bounce through the nozzle. The term coupled emphasizes that these electrons are energetically coupled to the plasma source, as the source restores their energy losses after every bounce through the nozzle. A local maximum in U_{eff} acts as a barrier for coupled electrons, making a certain area of phase space downstream inaccessible to them. The second group of electrons that we call decoupled are the electrons that occupy the inaccessible areas. These electrons

bounce between the mirror and the rarefaction wave without returning to the plasma source, so that their energy losses accumulate with time. An injected electron becomes decoupled when it fails to go over the barrier and return to the source after being reflected by the rarefaction wave. This occurs as a result of the electron energy loss experienced during the reflection. The process is analogous to what happens when a ball elastically rebounds from a retracting wall and loses some of its kinetic energy. It is important to point out that the electron magnetic moment remains conserved.

The energy lost by an electron in a single reflection from the rarefaction wave is relatively small compared to its total energy because the wave evolution is adiabatic. For a coupled electron, the energy losses are fully restored by the plasma source after every bounce. This enables us to treat both the magnetic moment μ and the total energy

$$\varepsilon \equiv \frac{m_e v^2}{2} - |e|\varphi \tag{6}$$

of a coupled electron as conserved quantities. For a decoupled electron, the energy losses gradually accumulate over time and thus the conserved quantities are the magnetic moment μ and the adiabatic invariant

$$I = \frac{1}{2\pi} \oint m_e v_\parallel dz. \tag{7}$$

In Eq. (7), $v_\parallel$ is the component of the electron velocity parallel to the magnetic field and the integration is performed over a single bounce period. The conservation of I for the decoupled electrons adequately describes their adiabatic cooling.

In order to to derive an explicit expression for n_e in Eq. (3), we need to express the electron distribution function f_e in terms of the given distribution of injected electrons f_0. As a consequence of the plasma's adiabatic expansion, the electron distribution function is nearly symmetric with respect to the longitudinal electron velocity $v_\parallel$ and we can therefore neglect its small asymmetry when calculating the electron density. The given distribution of injected electrons f_0 specifies f_e at the nozzle entrance only for $v_\parallel \geq 0$, but the symmetry of f_e means that $f_e(v_\parallel, v_\perp) = f_0(|v_\parallel|, v_\perp)$ for both signs of $v_\parallel$. This function describes both the injected and returning electrons. Since all electrons at the nozzle entrance are coupled electrons, we express f_e in terms of the conserved quantities μ and ε, such that $f_e = f_0(\varepsilon, \mu)$. This distribution is preserved by the Vlasov equation during the electron motion through the nozzle. We thus conclude that the expression $f_e = f_0(\varepsilon, \mu)$ is valid in all areas of phase

space accessible to the coupled electrons. In the case of decoupled electrons, the distribution function is preserved by the Vlasov equation if expressed in terms of I and μ. A direct way of expressing f_e in terms of I would obviously require the knowledge of the time evolution of $\varphi(z;t)$ in the entire flow downstream from the mirror throat. However, there is an easier way to deal with this problem.

Let us pick a value of μ with a non-monotonic profile of U_{eff}. The time-dependent part of the flow is gradually moving away from the mirror and, eventually, the barrier produced by U_{eff} becomes stationary. From this moment on, only injected electrons with the same energy $\varepsilon = \varepsilon_*(\mu)$ become decoupled, where $\varepsilon_*(\mu)$ is the height of the barrier. The distribution function of these electrons is constant in time, $f_e = f_0[\varepsilon_*(\mu), \mu]$. However, the adiabatic invariant corresponding to $\varepsilon = \varepsilon_*(\mu)$ increases with time as a result of the flow expansion. This means that the distribution function of the electrons, that become decoupled after the barrier became stationary, is independent of I. As the flow expansion continues and the decoupled population grows, the fraction of the electrons that became decoupled during the formation of the barrier diminishes. We can then safely neglect this transiently-formed population when constructing an asymptotic solution ($t \to +\infty$). The decoupled electrons gradually cool down losing energy and fill up the area of phase space inaccessible to the coupled electrons with the same μ. Therefore all decoupled electrons with the same magnetic moment μ have the same distribution function, $f_e = f_0[\varepsilon_*(\mu), \mu]$, in the asymptotic solution.

The electron density n_e can now be calculated as a sum of coupled and decoupled electron densities [15]. The resulting general expression for n_e involves a double integral over ε and μ. However it can be reduced to a single integral over energies if the distribution of injected electrons is independent of μ. This simplification applies conveniently to the particular case of an incoming flow with Maxwellian electrons discussed in Sec. III D.

A. Expressions for electron density

Upstream from the nozzle throat, U_{eff} is a monotonic function of z for all magnetic moments and the flow contains only coupled electrons. For a given magnetic moment μ, the lowest possible energy is $\varepsilon = U_{\text{eff}}$, which is equivalent to the condition $v_\parallel = 0$. As shown in Fig. 3, the constraint $\varepsilon \geq U_{\text{eff}}$ defines a boundary of the phase space area occupied by

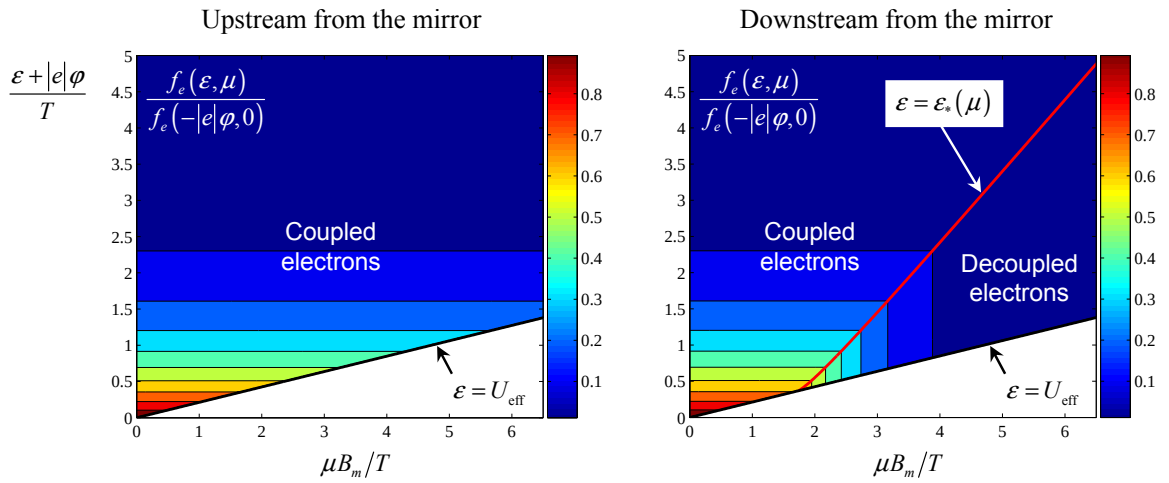

FIG. 3: Electron distribution function upstream (left contour plot) and downstream (right contour plot) from the nozzle throat for the case of injected Maxwellian electrons with temperature T. The left contour plot corresponds to $B/B_m \approx 0.21$ and $|e|\varphi/T \approx 0.49$, where B_m is the magnetic field at the mirror. The electrostatic potential is defined such that $\varphi = \varphi_m = 0$ at the mirror. The right contour plot corresponds to $B/B_m \approx 0.21$ and $|e|\varphi/T \approx -1.66$.

coupled electrons at a given axial location. The boundary depends only on the local values of φ and B. The electron density is then given by

$$n_e = \pi B \left(\frac{2}{m_e}\right)^{3/2} \int_0^\infty d\mu \int_{U_{\text{eff}}}^\infty \frac{f_0(\varepsilon)d\varepsilon}{\sqrt{\varepsilon - U_{\text{eff}}}}, \tag{8}$$

where the conventional expression for n_e in terms of integrals over $v_\perp$ and $v_\parallel$ has been replaced by integrals over ε and μ using definitions (4), (5) and

$$\varepsilon = \frac{m_e v^2}{2} - |e|\varphi = \frac{m_e v_\parallel^2}{2} + U_{\text{eff}}. \tag{9}$$

We change the order of integration in Eq. (8) and evaluate the resulting integral over μ, which does not involve f_0, to find that

$$n_e = 2\pi \left(\frac{2}{m_e}\right)^{3/2} \int_{-|e|\varphi}^\infty f_0(\varepsilon)\sqrt{\varepsilon + |e|\varphi}\, d\varepsilon. \tag{10}$$

Downstream from the nozzle throat, the flow electrons also occupy the phase space area bounded by the curve $\varepsilon = U_{\text{eff}}$. However the electron distribution function in this area is different from the upstream case because decoupled electrons occupy a part of the area,

as illustrated in Fig. 3. Unlike the boundary of the electron population that depends on the local values of φ and B, the curve separating coupled and decoupled electrons (the separatrix) depends on the entire profile of φ upstream. We have already introduced $\varepsilon_*(\mu)$ as the height of a barrier in U_{eff} for a given value of the magnetic moment μ. It follows directly from the definition of $\varepsilon_*(\mu)$ and Fig. 3 that the separatrix is specified by the equation $\varepsilon = \varepsilon_*(\mu)$, where μ runs through all magnetic moments that have a barrier in the effective potential upstream from the current axial location. In order to find $\varepsilon = \varepsilon_*(\mu)$, one has to solve these two equations:

$$\varepsilon = \mu B - |e|\varphi, \tag{11}$$

$$\mu \frac{dB}{d\varphi} - |e| = 0. \tag{12}$$

Equation (11) gives the energy of injected electrons with magnetic moment μ that become decoupled from the plasma source after reflecting off the rarefaction wave. Equation (12) is the condition $dU_{\text{eff}}/d\varphi = 0$, which is equivalent to $dU_{\text{eff}}/dz = 0$, because φ is a monotonic function of z and the guiding magnetic field can be expressed at every time instant in terms of φ. Equation (12) relates B and φ at the location where the barrier is the highest for the given magnetic moment. Therefore one way to resolve Eqs. (11) and (12) is to express B in terms of φ, solve Eq. (12) for $\varphi(\mu)$, and use the resulting function in Eq. (11) to express the right-hand side in terms of μ and find $\varepsilon = \varepsilon_*(\mu)$. Equivalently, Eqs. (11) and (12) can be used to find $\mu = \mu_*(\varepsilon)$.

As shown in Fig. 3, the separatrix crosses the $v_\parallel = 0$ boundary at $\mu = \mu_t$. The value of μ_t is given by Eq. (12),

$$\mu_t = \frac{|e|}{dB/d\varphi}, \tag{13}$$

where the right-hand side must be calculated at the current axial location using the local values of the magnetic field and the electrostatic potential. Indeed, at the intersection point, Eqs. (11) and (12) must be compatible with the equation that specifies the boundary of the electron population, $\varepsilon = U_{\text{eff}}$. The equation $\varepsilon = U_{\text{eff}}$ is identical to Eq. (11), but it involves local values of B and φ. As a result, the compatibility of the three equations requires us to use the local value of $dB/d\varphi$ in Eq. (12) as well and we immediately arrive to Eq. (13).

We now find that, for a given function $\varepsilon = \varepsilon_*(\mu)$, the expression for the electron density downstream from the nozzle throat is

$$\begin{aligned} n_e \;=\; & \pi B \left(\frac{2}{m_e}\right)^{3/2} \int_0^{\mu_t} d\mu \int_{U_{\rm eff}}^{\infty} \frac{f_0(\varepsilon) d\varepsilon}{\sqrt{\varepsilon - U_{\rm eff}}} \\ & + \; \pi B \left(\frac{2}{m_e}\right)^{3/2} \int_{\mu_t}^{\infty} d\mu \left[\int_{\varepsilon_*(\mu)}^{\infty} \frac{f_0(\varepsilon) d\varepsilon}{\sqrt{\varepsilon - U_{\rm eff}}} + \int_{U_{\rm eff}}^{\varepsilon_*(\mu)} \frac{f_0[\varepsilon_*(\mu)] d\varepsilon}{\sqrt{\varepsilon - U_{\rm eff}}} \right]. \end{aligned} \tag{14}$$

The integrals in Eq. (14) are written according to Fig. 3 that illustrates how the "inaccessible" areas of phase space fill up with decoupled electrons. Equation (14) is similar to Eq. (6) in Ref. [15]. Integrating by parts over energy, we transform Eq. (14) to

$$n_e \;=\; -2\pi B \left(\frac{2}{m_e}\right)^{3/2} \left[\int_0^{\mu_t} d\mu \int_{U_{\rm eff}}^{\infty} d\varepsilon + \int_{\mu_t}^{\infty} d\mu \int_{\varepsilon_*(\mu)}^{\infty} d\varepsilon \right] \frac{df_0(\varepsilon)}{d\varepsilon} \sqrt{\varepsilon - U_{\rm eff}}. \tag{15}$$

To take advantage of the fact that f_0 is independent of μ, we change the order of integration in Eq. (15):

$$\begin{aligned} n_e \;=\; & -2\pi B \left(\frac{2}{m_e}\right)^{3/2} \int_{-|e|\varphi}^{U_{\rm eff}(\mu_t)} \frac{df_0(\varepsilon)}{d\varepsilon} d\varepsilon \int_0^{(\varepsilon+|e|\varphi)/B} \sqrt{\varepsilon - U_{\rm eff}} d\mu \\ & -2\pi B \left(\frac{2}{m_e}\right)^{3/2} \int_{U_{\rm eff}(\mu_t)}^{\infty} \frac{df_0(\varepsilon)}{d\varepsilon} d\varepsilon \int_0^{\mu_*(\varepsilon)} \sqrt{\varepsilon - U_{\rm eff}} d\mu, \end{aligned} \tag{16}$$

where $\mu = \mu_*(\varepsilon)$ is the function specified by Eqs. (11) and (12) as described above. After integrating over μ in Eq. (16), we find that

$$\begin{aligned} n_e \;=\; & \frac{4}{3}\pi \left(\frac{2}{m_e}\right)^{3/2} \int_{\mu_t B - |e|\varphi}^{\infty} \frac{df_0(\varepsilon)}{d\varepsilon} \left[\varepsilon + |e|\varphi - \mu_*(\varepsilon) B\right]^{3/2} d\varepsilon \\ & - \; \frac{4}{3}\pi \left(\frac{2}{m_e}\right)^{3/2} \int_{-|e|\varphi}^{\infty} \frac{df_0(\varepsilon)}{d\varepsilon} \left[\varepsilon + |e|\varphi\right]^{3/2} d\varepsilon. \end{aligned} \tag{17}$$

A comparison with the upstream case [see Eq. (10)] reveals that the second term in Eq. (17) is the same contribution that is given by Eq. (10) when the flow contains only coupled electrons. The first term in Eq. (17) accounts for the fact that the area of phase space below the separatrix is filled with decoupled electrons.

Equation (17) is a general expression for the electron density that works both near the

mirror and in the region where the magnetic field is low. In the low magnetic field region, the expression for n_e can be simplified by expanding the right-hand side of Eq. (17) with respect to B and keeping only the linear terms of the expansion:

$$n_e \;=\; -2\pi B \left(\frac{2}{m_e}\right)^{3/2} \int_{-|e|\varphi}^{\infty} \frac{df_0(\varepsilon)}{d\varepsilon} \mu_*(\varepsilon) \sqrt{\varepsilon + |e|\varphi}\, d\varepsilon. \tag{18}$$

To obtain Eq. (18), we took into account that, by definition, the square bracket in the first integral in Eq. (17) vanishes at the lower limit.

B. Steady flow equations

In a steady-state flow, Eqs. (1) and (2) readily reduce to a single algebraic equation,

$$\frac{B}{B_m} \;=\; \frac{n}{n_m} \sqrt{1 - \frac{|e|\varphi}{m_i V_m^2/2}}, \tag{19}$$

where the subscript m marks quantities at the mirror (nozzle throat) and the electrostatic potential is defined such that $\varphi_m = 0$.

Equations (19) and (10) form a closed system for the plasma flow upstream from the magnetic mirror and yield a single equation that relates B and φ:

$$\frac{B}{B_m} \;=\; \sqrt{1 - \frac{|e|\varphi}{m_i V_m^2/2}} \left[\int_0^{\infty} f_0(\varepsilon) \sqrt{\varepsilon}\, d\varepsilon\right]^{-1} \int_{-|e|\varphi}^{\infty} f_0(\varepsilon) \sqrt{\varepsilon + |e|\varphi}\, d\varepsilon. \tag{20}$$

In the considered nozzle configuration, the steady-state solution $B = B(\varphi)$ must be such that $dB/d\varphi < 0$ upstream from the mirror and $dB/d\varphi > 0$ downstream from the mirror. The derivative must vanish at the nozzle throat, where $\varphi = 0$, and this condition determines V_m. It follows from Eq. (20) that

$$V_m \;=\; \sqrt{\frac{2}{m_i} \int_0^{\infty} f_0(\varepsilon) \varepsilon^{1/2} d\varepsilon \Big/ \int_0^{\infty} f_0(\varepsilon) \varepsilon^{-1/2} d\varepsilon}. \tag{21}$$

Equations (20) and (21) explicitly determine the relation between B and φ upstream from the mirror. Note that V_m is the local speed of sound and the mirror throat is the location where the sub- to supersonic transition takes place.

The steady part of the plasma flow downstream from the mirror is described by Eqs. (19) and (17). They readily combine into to an integral equation that relates B and φ,

$$\frac{B}{B_m} = \sqrt{1-\frac{|e|\varphi}{m_i V_m^2/2}}\left[\int_0^\infty f_0(\varepsilon)\sqrt{\varepsilon}d\varepsilon\right]^{-1} \times \left[\frac{2}{3}\int_{\frac{|e|B}{dB/d\varphi}-|e|\varphi}^\infty \frac{df_0(\varepsilon)}{d\varepsilon}\left[\varepsilon+|e|\varphi-\mu_*(\varepsilon)B\right]^{3/2}d\varepsilon + \int_{-|e|\varphi}^\infty f_0(\varepsilon)\sqrt{\varepsilon+|e|\varphi}d\varepsilon\right], \quad (22)$$

where we explicitly used the definition of μ_t given by Eq. (13). Equation (22) should be solved together with the equations for $\mu_*(\varepsilon)$ [see Eqs. (11) and (12)] to find a steady-state solution for a given distribution $f_0(\varepsilon)$ of injected electrons. In general, this step needs to be done numerically. In Sec. III D, we solve these equations to construct a solution for the case of incoming Maxwellian electrons.

The flow in the expanding part of the nozzle is supersonic and, therefore, the boundary between the steady flow described by Eq. (22) and the time-dependent flow is gradually moving downstream. At $t \to +\infty$, the boundary is located in a low magnetic field region. To find an equation for the asymptotic value of the electrostatic potential φ_b at the boundary, we substitute the low-field approximation for n_e given by Eq. (18) into Eq. (19), which yields

$$B_m\sqrt{1-\frac{|e|\varphi_a}{m_i V_m^2/2}}\int_{-|e|\varphi_b}^\infty \frac{df_0(\varepsilon)}{d\varepsilon}\mu_*(\varepsilon)\sqrt{\varepsilon+|e|\varphi_b}d\varepsilon = -\int_0^\infty f_0(\varepsilon)\sqrt{\varepsilon}d\varepsilon. \quad (23)$$

Equation (23) determines the asymptotic drop of the ambipolar potential between the nozzle throat and the rarefaction wave. The fact that φ_b has an asymptotic value indicates that the steady-state solution in the low-field region describes a diverging plasma flow without an ambipolar electric field. In other words, plasma ions move ballistically through the steady-state region before they enter the rarefaction wave.

Clearly, the drop of the ambipolar potential φ_b in the the steady flow is insufficient to reflect all the electrons moving downstream. The steady-state solution then has to be matched to a rarefaction wave (time-dependent part of the flow) that accommodates a part of the total potential drop needed to reflect all the electrons and to keep electrons and ions together in the expanding plume.

C. Rarefaction wave in low-field region

The rarefaction wave, which is the time dependent part of the flow, is described by Eqs. (1) - (3). In an asymptotic solution ($t \to +\infty$), the rarefaction wave is far away from the nozzle throat in a region with a low magnetic field. It is then appropriate to use the low-field expression (18) for the electron density in Eq. (2).

To make our further expressions more compact, we introduce new variables:

$$N \equiv \frac{nB_m}{n_m B}, \tag{24}$$

$$\tau \equiv t\sqrt{\frac{T}{m_i}}, \tag{25}$$

$$u \equiv V\sqrt{\frac{m_i}{T}}, \tag{26}$$

$$\phi \equiv -\frac{|e|\varphi}{T}, \tag{27}$$

where T is a characteristic electron energy that will be taken to be equal to the electron temperature in Sec. III D. The values of N, u, and ϕ at the boundary between the rarefaction wave and the steady flow are

$$N_b = \left[1 - \frac{|e|\varphi_b}{m_i V_m^2/2}\right]^{-1/2}, \tag{28}$$

$$u_b = \sqrt{\frac{m_i}{T}}\frac{V_m}{N_b}, \tag{29}$$

$$\phi_b \equiv -\frac{|e|\varphi_b}{T}, \tag{30}$$

where φ_b is the solution of Eq. (23). Equations (1) and (2) now take the following form:

$$\frac{\partial u}{\partial \tau} + u\frac{\partial u}{\partial z} = \frac{\partial \phi}{\partial z}, \tag{31}$$

$$\frac{\partial N}{\partial \tau} + u\frac{\partial N}{\partial z} = -N\frac{\partial u}{\partial z}, \tag{32}$$

with

$$N = -\left[\int_0^\infty f_0(xT)\sqrt{x}dx\right]^{-1} \int_\phi^\infty \frac{df_0(xT)}{dx}\frac{\mu_*(xT)B_m}{T}\sqrt{x-\phi}dx. \tag{33}$$

As τ increases, the values of z in the rarefaction wave become large compared to the nozzle length. This indicates that, at $\tau \to +\infty$, the solution of Eqs. (31) and (32) will take a universal self-similar form independent of the nozzle length. We therefore construct the rarefaction wave by assuming that $u = u(\phi)$, $N = N(\phi)$, and $\phi(z,\tau) = \phi(\xi)$, where $\xi \equiv z/\tau$. Under these assumptions, Eqs. (31) and (32) yield the following two relations:

$$\left(\frac{du}{d\phi}\right)^2 = -\frac{1}{N}\frac{dN}{d\phi}, \tag{34}$$

$$\xi = u - \left(\frac{du}{d\phi}\right)^{-1}. \tag{35}$$

We use Eq. (33) to express the right-hand side of Eq. (34) in terms of ϕ and then integrate the resulting equation to find

$$u(\phi) = u_a + \int_{\phi_a}^{\phi} \left[\int_{\phi'}^{\infty} \frac{df_0(xT)}{dx}\frac{\mu_*(xT)dx}{2\sqrt{x-\phi'}} \Big/ \int_{\phi'}^{\infty} \frac{df_0(xT)}{dx}\mu_*(xT)\sqrt{x-\phi'}dx\right]^{1/2} d\phi'. \tag{36}$$

Equation (36) determines u as a function of ϕ and we can now use Eq. (35) to determine ξ as a function of ϕ as well,

$$\xi(\phi) = u(\phi) - \left[\int_{\phi}^{\infty} \frac{df_0(xT)}{dx}\frac{\mu_*(xT)dx}{2\sqrt{x-\phi}} \Big/ \int_{\phi}^{\infty} \frac{df_0(xT)}{dx}\mu_*(xT)\sqrt{x-\phi}dx\right]^{-1/2}. \tag{37}$$

Equations (36) and (37) implicitly determine $\phi(\xi)$ for a given function f_0. Once $\phi(\xi)$ is determined, Eqs. (33) and (36) should be used to find $N(\xi)$ and $u(\xi)$.

At the boundary between the rarefaction wave and the steady flow, we have $\xi = \xi(\phi_b)$, where $\xi(\phi_b)$ should be calculated using Eq. (37). It follows from the definition of ξ that the asymptotic axial location of the boundary is $z = z_b(t) = \xi(\phi_b)\sqrt{T/m_i}t$.

D. Nozzle thrust and power

In this section we apply the procedure outlined in Secs. III B and III C to find the expanding plume solution for the case of injected Maxwellian electrons, with

$$f_0(\varepsilon) = \left(\frac{m_e}{2\pi T}\right)^{3/2} n_m \exp(-\varepsilon/T), \tag{38}$$

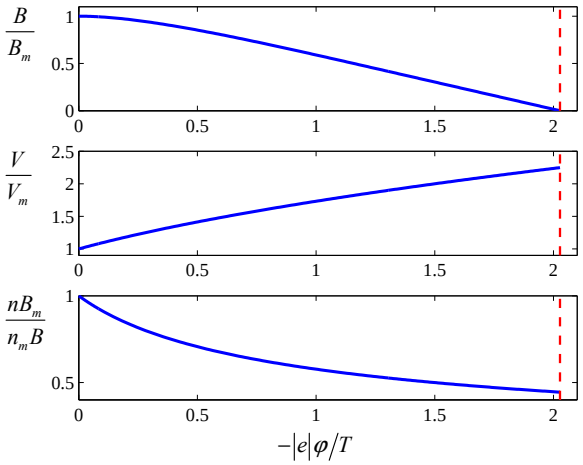

FIG. 4: Steady-state part of the solution for the case of injected Maxwellian electrons with temperature T.

where T is the electron temperature. Using Eq. (20), we find the relation between B and φ upstream from the nozzle throat analytically:

$$\frac{B}{B_m} = \sqrt{1 - 2\frac{|e|\varphi}{T}} \exp\left(\frac{|e|\varphi}{T}\right), \tag{39}$$

where it is taken into account that, according to Eq. (21),

$$V_m = \sqrt{T/m_i} \tag{40}$$

for f_0 given by Eq. (38).

We solve Eq. (22) numerically to find $B = B(\varphi)$ downstream from the nozzle throat in the stead-state part of the flow. The numerical procedure that we use is outlined at the end of this section after we describe the results. The asymptotic solution ($t \to +\infty$) of Eq. (22) together with the corresponding profiles of V and n/B are shown in Fig. 4. The guiding magnetic field vanishes at $\varphi \approx -2.03T/|e|$, as indicated by a dashed line. Therefore the drop of the electrostatic potential downstream from the mirror throat in the steady flow is $\varphi_b \approx -2.03T/|e|$.

It is instructive to compare the solution shown in Fig. 4 with the solution that one obtains under the assumption that the entire electron distribution is Maxwellian downstream from the magnetic mirror. The latter one is given by Eq. (39), so that the electrostatic potential diverges downstream from the mirror throat, with $\varphi \to -\infty$ for $B \to 0$. Consequently,

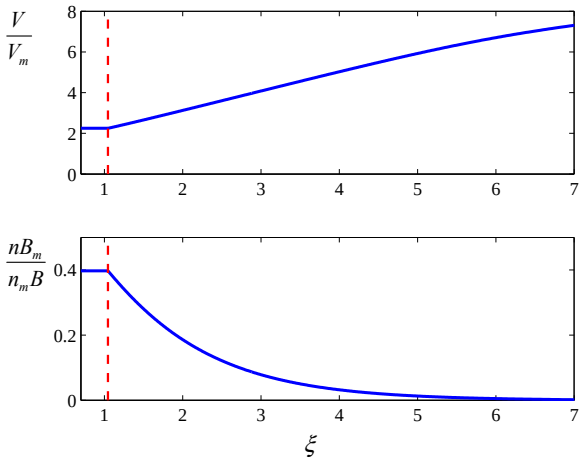

FIG. 5: Flow velocity and density in the rarefaction wave for the case of injected Maxwellian electrons. The red line indicates the boundary between the rarefaction wave and the steady flow shown in Fig. 4.

the ion velocity also diverges in this asymptotic solution. The dramatic difference in ion acceleration between the two cases results from the difference in the electron distribution, which emphasizes the importance of the kinetic description.

Figure (3) shows the electron distribution at two different axial locations: upstream (left panel) and downstream (right panel) from the mirror. In the upstream case (left panel), the distribution is purely Maxwellian. The downstream case differs only in the area below the separatrix that is now filled with decoupled electrons. The distribution function in this area is less than the Maxwellian distribution for the same values of ε and μ. Thus the phase space below the separatrix is underpopulated compared to the case of a purely Maxwellian distribution.

The steady-state solution shown in Fig. 4 matches to a rarefaction wave at $\varphi = \varphi_b$. We use Eqs. (33), (36), and (37) to find the rarefaction wave solution shown in Fig. 5 for the distribution of injected electrons given by Eq. (38). The rarefaction wave accommodates the drop of the ambipolar potential necessary to reflect all those electrons that travel past the steady part of the flow, as evident from the lower panel of Fig. 4. The same field that slows down the electrons, provides ions with additional acceleration (see upper panel of Fig. 5). The inner wave front shown with a red dotted line is a sonic wave propagating upstream with respect to the ion flow. There is a constant influx of ions into the rarefaction wave through the wave front and, in the asymptotic solution, the wave contains 42% of all ions that are located downstream from the nozzle throat.

Using the asymptotic solutions for the steady and time-dependent parts of the flow, we find the thrust produced by the nozzle:

$$\frac{dP}{dt} \approx 2.48 \cdot n_m T S_m, \tag{41}$$

where P is the total momentum of the flow, and n_m and S_m are ion density and the flow cross-section at the mirror throat. The total momentum is the ion momentum because the electron momentum is negligible in the adiabatic flow being considered. The power needed to produce this thrust is

$$\frac{dK}{dt} \approx 4.48 \cdot n_m T \sqrt{T/m_i} S_m, \tag{42}$$

where K is the total kinetic energy of the flow that includes both the ion (K_i) and electron (K_e) contributions. The ion contribution to the power turns out to be the dominant one,

$$\frac{dK_i/dt}{dK_e/dt} \approx 5.14. \tag{43}$$

We conclude this section with a brief discussion of the procedure used to solve Eq. (22). Our first step is to differentiate both sides of Eq. (22) with respect to φ and rearrange the resulting equation to take the form $dB/d\varphi = G(B, \varphi, dB/d\varphi)$, where $dB/d\varphi$ enters the right-hand side only through the limits of integration. It is important to point out that the second derivative of B is not present in this equation. The structure of the rearranged equation then allows us to solve it iteratively, using the following algorithm:

$$B^k(\varphi) = B_m + \int_0^{\varphi} G\left[\varphi', B^{k-1}(\varphi'), \frac{d}{d\varphi'} B^{k-1}(\varphi')\right] d\varphi', \tag{44}$$

where the superscript k represents the number of the iteration. The right-hand side involves the function $\mu_*(\varepsilon)$ that should be calculated using Eqs. (11) and (12), with $B = B^{k-1}$ and $dB/d\varphi = dB^{k-1}/d\varphi$.

In order to achieve convergence, we start with a short interval, $\varphi \in [0, \varphi_1]$, such that $B(\varphi_1)/B_m$ calculated using Eq. (39) is close to unity. For the first iteration, we use B^0 and $dB^0/d\varphi$ evaluated using Eq. (39). Once the desired convergence is achieved on the initial interval $\varphi \in [0, \varphi_1]$, we expand it to $\varphi \in [0, \varphi_2]$, where $\varphi_2 < \varphi_1$. For the first iteration on the new interval, we use the already known solution at $\varphi \in [0, \varphi_1]$ as B^0 and $dB^0/d\varphi$. We

use the cubic spline extrapolation of the solution at $\varphi \in [0, \varphi_1]$ to calculate B^0 and $dB^0/d\varphi$ at $\varphi \in (\varphi_1, \varphi_2]$. We apply the iterative procedure for the entire interval $\varphi \in [0, \varphi_2]$ until we achieve convergence once again. We then extend the interval and repeat the steps described above. This procedure allows us to gradually extend the interval such that the magnetic field at the end of the interval is much less than B_m. The next step is to extrapolate the solution and find $\varphi = \varphi_b$ where $B = 0$. This value should be close to the one that one finds from Eq. (23) using $\mu_*(\varepsilon)$ from the iterative procedure. It should be pointed out that the numerical iterative procedure does not allow us to find φ_b directly, even though $dB/d\varphi$ is finite at $\varphi = \varphi_b$. The reason is that the analytical expression for $G(B, \varphi, dB/d\varphi)$ is a fraction, whose numerator and denominator both vanish as $\varphi \to \varphi_b$.

IV. DISCUSSION

Besides the apparent similarity between the magnetic nozzle and the gas dynamic de Laval nozzle, there is also an important difference between the two. The gas jet in the de Laval nozzle is adiabatic whereas plasma electrons are isothermal due to very high electron thermal conductivity. The highly mobile electrons can deliver virtually unlimited power from the plasma source to the outgoing ion plume. As a result, a formally constructed steady-state ambipolar plasma flow with isothermal Maxwellian electrons produces infinite thrust and requires infinite power, which is clearly unphysical. This predicament follows immediately from the fact that the particle flux is constant within the magnetic flux tube whereas the ambipolar potential grows to infinity downstream in the case of isothermal Maxwellian electrons, leading to unlimited acceleration of the ions. It is noteworthy that the barrier in the effective potential energy for the electrons limits the electron heat flux to the outgoing plume and thereby gives finite and physically reasonable values for the thrust and power shown by Eqs. (41) and (42).

Another interesting consequence of electron decoupling is that there is an extended area in the plasma flow where the ambipolar electric field nearly vanishes and the ions move downstream ballistically without acceleration despite the decrease in the plasma density. This would not be possible in a plasma with isothermal Maxwellian electrons where any plasma density gradient would automatically create an ambipolar electric field.

The assumption that electrons are collisionless in the flow requires that their mean free

path remains greater than the plume length during plasma expansion. For coupled electrons, this condition remains always satisfied, provided that it is satisfied early in time. Indeed, the local value of the mean free path λ, which is inversely proportional to plasma density, increases as l^2 with the length of the plume l. Therefore the ratio of λ/l increases as l as the plume expands, meaning that the electrons do not become more collisional over time. The collisionality constraint is somewhat more restrictive for the decoupled electrons. It requires the time-scale of adiabatic cooling to be shorter than the Coulomb scattering time. A decoupled electron needs roughly $\sqrt{m_i/m_e}$ reflections from the rarefaction wave in order to lose its energy. This leads to the condition $\lambda/l \gg \sqrt{m_i/m_e}$ rather than $\lambda/l \gg 1$ for the coupled electrons. Still, the role of collisionality does not increase over time for the decoupled electrons.

We thus conclude that Coulomb collisions do not affect the electron distribution function in the plume in any significant way if the plume is initially collisionless. The only candidate mechanism to alter the collisionless solution described in this paper would be an instability of the anisotropic non-Maxwellian electrons. A complete stability assessment goes beyond the scope of this work. Yet, a preliminary analysis shows that an electron distribution with an empty hole in the decoupled area of phase space turns out to be strongly unstable with respect to excitation of plasma density fluctuation. The underlying reason is that the absence of slow electrons in the distribution function changes the sign of electron compressibility, so that ion fluctuation grow aperiodically instead of propagating as sound waves. The population of decoupled electrons that builds up naturally due to the rarefaction wave suppresses this particular instability, which resonates with the old notion that nature abhors a vacuum.

V. SUMMARY

We have considered two systems with intrinsically non-Maxwellian electron distributions: an expanding laser-irradiated nanoplasma (micro-cluster) and a supersonic jet coming out of a magnetic nozzle. The kinetic analysis of these two problems demonstrates how the deviation from the Maxwellian distribution fundamentally alters ion acceleration compared to a model that postulates a Maxwellian electron distribution in the entire flow. The problem of a laser-irradiated nanoplasma highlights the critical role of hot non-thermal electrons in

the ion acceleration process, whereas the magnetic nozzle problem shows the important role of the moving plasma edge in the distortion of the electron distribution.

The key points of the expanding nanoplasma problem are

- the laser field can create a two-component electron distribution with a cold majority and a hot minority,
- co-existence of the two electron populations within the same ion background leads to a breakdown of quasineutrality at the cluster edge,
- hot electrons maintain a steady-state double layer at the cluster edge during the expansion,
- ions pre-accelerate in the double layer to supersonic velocities, gaining as much as half of their final energy, and then their acceleration continues in the rarefaction wave.

The key points of the magnetic nozzle problem are

- the supersonic flow downstream from the magnetic mirror consists of a steady-state part and a rarefaction wave at the leading edge of the expanding plasma,
- the magnetic mirror together with the rarefaction wave produce a population of decoupled electrons in the "inaccessible" area of phase space,
- the "inaccessible" area is underpopulated compared to the case of a purely Maxwellian distribution,
- the values of the nozzle thrust and required power are finite as opposed to the diverging values predicted by a model postulating a Maxwellian electron distribution in the entire flow.

Acknowledgments

This work is supported by the U.S. Department of Energy under Contract No. DE-FG02-04ER-54742. The authors thank Mikhail Tushentsov for his constructive comments

regarding the numerical algorithm.

---

[1] E. Leer, E. Holzer, T. Fla, Space Sci. Rev. **33**, 161 (1982).

[2] F. R. Chang-Daz, Sci. Am. **283**, 90 (2000).

[3] G. Hairapetian and R. L. Stenzel, Phys. Rev. Lett. **61**, 1607 (1988).

[4] T. Ditmire, J. Zweiback, V. P. Yanovsky, T. E. Cowan, G. Hays, and K. B. Wharton, Nature (London) **398**, 489 (1999).

[5] S. P. Hatchett, C. G. Brown, T. E. Cowan, E. A. Henry, J. S. Johnson, M. H. Key, J. A. Koch, A. B. Langdon, B. F. Lasinski, R. W. Lee, A. J. Mackinnon, D. M. Pennington, M. D. Perry, T. W. Phillips, M. Roth, T. C. Sangster, M. S. Singh, R. A. Snavely, M. A. Stoyer, S. C. Wilks, and K. Yasuike, Phys. Plasmas **7**, 2076 (2000)

[6] A. V. Gurevich, L. V. Pariiskaya, and L. P. Pitaevskii, Zh. Eksp. Teor. Fiz. **49**, 647 (1965) [Sov. Phys. JETP **22**, 449 (1966)].

[7] J. E. Crow, P. L. Auer, and J. E. Allen, J. Plasma Phys. **14**, 65 (1975).

[8] J. S. Pearlman and R. L. Morse, Phys. Rev. Lett. 40, 1652 (1978).

[9] J. Denavit, Phys. Fluids 22, 1384 (1979).

[10] M. A. True, J. R. Albritton, and E. A. Williams, Phys. Fluids **24**, 1885 (1981).

[11] A. V. Gurevich and A. P. Meshcherkin, Zh. Eksp. Teor. Fiz. **53**, 1810 (1981) [Sov. Phys. JETP **53**, 937 (1981)].

[12] P. Mora, Phys. Rev. Lett. **90**, 185002 (2003).

[13] V. F. Kovalev and V. Yu. Bychenkov, Phys. Rev. Lett. **90**, 185004 (2003).

[14] B. N. Breizman and A. V. Arefiev, Phys. Plasmas **14**, 073105 (2007).

[15] A. V. Arefiev and B. N. Breizman, Phys. Plasmas **15**, 042109 (2008).

[16] L. D. Landau and E. M. Lifshitz, *Fluid Mechanics*, 2nd ed. (Pergamon, Oxford, 1979), p. 348.

[17] P. G. Mikellides, P. J. Turchi, and I. G. Mikellides, J. Propul. Power **18**, 146 (2002); I. G. Mikellides, P. G. Mikellides, P. J. Turchi, and T. M. York, J. Propul. Power **18**, 152 (2002).

[18] M. Liemohn and G. Khazanov, Phys. Plasmas **5**, 580 (1998).

[19] F. Brunel, Phys. Rev. Lett. **59**, 52 (1987).

[20] F. Brunel, Phys. Fluids **31**, 2714 (1988).

[21] Y. Kishimoto, T. Masaki, and T. Tajima, Phys. Plasmas **9**, 589 (2002).

[22] B. N. Breizman and A. V. Arefiev, Plasma Phys. Rep. **29**, 593 (2003).

[23] T. M. Antonsen, T. Taguchi, A. Gupta, J. Palastro, and H. M. Milchberg, Phys. Plasmas 12, 056703 (2005).

[24] B. N. Breizman, A. V. Arefiev, and M. V. Fomytskyi, Phys. Plasmas **12**, 056706 (2005).